Optical Fiber Technology 72 (2022) 103000

Contents lists available at ScienceDirect

Optical Fiber Technology

journal homepage: www.elsevier.com/locate/yofte

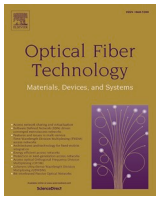

Invited Papers

Recent advances in fiber optic sensors for respiratory monitoring

Cong Zhao [a,b,c], Dan Liu [b,c], Gaixia Xu [d], Jiangtao Zhou [e], Xuming Zhang [f], Changrui Liao [b,c,*], Yiping Wang [a,b,c]

[a] Laboratory of Artificial Intelligence and Digital Economy (SZ), Shenzhen 518000, China
[b] Key Laboratory of Optoelectronic Devices and Systems of Ministry of Education and Guangdong Province, College of Physics and Optoelectronic Engineering, Shenzhen University, Shenzhen 518060, China
[c] Shenzhen Key Laboratory of Photonic Devices and Sensing Systems for Internet of Things, Guangdong and Hong Kong Joint Research Centre for Optical Fiber Sensors, Shenzhen University, Shenzhen 518060, China
[d] Guangdong Key Laboratory for Biomedical Measurements and Ultrasound Imaging, School of Biomedical Engineering, Health Science Center, Shenzhen University, Shenzhen 518055, China
[e] Laboratory of Physics of Living Matter, IPHYS, Ecole Polytechnique Fédérale de Lausanne (EPFL), CH-1015 Lausanne, Switzerland
[f] Department of Applied Physics, The Hong Kong Polytechnic University, Hong Kong SAR, China

ARTICLE INFO

Keywords:
Fiber optic sensors
Respiratory rate
Wearable sensor
Breath monitoring

ABSTRACT

There is a growing need to measure respiratory rate (RR) in a variety of applications, including in clinical and occupational settings, as well as during physical exercises. Fiber optic sensors (FOSs) is an attractive solution for wearable RR monitoring because of their small size, multiplexing capability, chemical inertness, and immunity to electromagnetic fields. Here, we review recent advances in FOSs for breath monitoring. We presented the sensing mechanisms of state-of-the-art sensors and analyze their advantages and disadvantages. We classified recently reported FOSs based on sensing principles and then critically analyze the strengths and weaknesses of representative recent works. Finally, we summarized the challenges and future prospects of breath FOSs, with the aim of applying them to real applications.

1. Introduction

There has been a growing demand for monitoring respiratory-related parameters in various applications, of which respiratory rate (RR) is probably the most valuable to measure. The RR, also known as breath per minute (bpm), is a physiological variable that reflects human ventilation. Normal RR for an adult at rest is approximately 12 to 20 bpm. Breath monitoring helps to understand health status in clinical use [1], for health and safety at work [2], and during physical activity [3].

A large body of clinical evidence suggests that RR is a very useful vital sign. RR can be regarded as an early indicator of a physiologically deteriorating condition [4]. For example, the RR can be used to predict cardiac arrest, to assess the prognosis of acute myocardial infarction [5], and as an important reference for intensive care unit admission [2]. In addition, RR is a predictor of numerous potentially serious adverse events, such as sleep apnea [6], respiratory depression in postoperative patients [7] and sudden infant death syndrome [8]. Alterations in RR have also been shown associated with diseases such as diabetic ketoacidosis, toxicological problems, shock, pain, sepsis, allergic reactions and dehydration [9].

RR can be used as a means of monitoring the health and safety of workers during their activities. Various wearable devices for monitoring RR have been developed and tested for workers with high levels of psychophysiological stress [10]. RR has been shown to be useful for the assessment of cognitive load, emotional stress, environmental challenges, pain and discomfort in workers [11].RR has also been used as a sensitive indicator of workload and is important for workers exposed to demanding tasks and significant responsibilities, including pilots, soldiers and surgeons [12]. In addition, RR is strongly influenced by body temperature [13] and can be used as an indicator of thermal stress, which is important for workers in hot environments, e. g., firefighters [13].

RR is a better marker of physical effort compared to the physiological variables traditionally used (e.g., oxygen uptake, blood lactate and heart rate) [3]. It is very sensitive to work rate changes that occur during intermittent exercise [3]. This fits with the intermittent nature of many

* Corresponding author at: Shenzhen Key Laboratory of Photonic Devices and Sensing Systems for Internet of Things, Guangdong and Hong Kong Joint Research Centre for Optical Fiber Sensors, Shenzhen University, Shenzhen 518060, China.
E-mail address: cliao@szu.edu.cn (C. Liao).

https://doi.org/10.1016/j.yofte.2022.103000
Received 1 April 2022; Accepted 19 July 2022
Available online 30 July 2022

physical activities such as basketball, football, and other team sports. Measuring RR during exercise has implications for other populations as well. For example, an altered RR is the indicator of dyspnea during exercise [14]. It is also a marker of exercise tolerance in patients with chronic obstructive pulmonary disease (COPD) [15].

In order to respond to the growing demand of techniques that non-invasively monitor human RR, various techniques are being developed, in which fiber optical sensors (FOSs) are probably the most promising type. FOSs are typically in small size with the capability of multiplexing and chemical inertness [16]. Compared with the traditional electronic sensors, FOSs are intrinsically immunity to electromagnetic fields. FOSs have been demonstrated with good linearity, rapid response, and excellent sensitivity [17]. Thus, FOSs is turned out to be very attractive for the application of RR monitoring.

In this review, we overview the recent developments on the FOS-based breath monitoring sensors, as shown in Fig. 1. The widely used techniques of FOSs for RR monitoring are addressed specifically: intensity-based, fiber grating and interferometer. Selected demonstrations that highlight their progress in RR monitoring are reviewed, categorized by their sensing principle. We also compare the response/recovery times, packaging solution, and capability to measure multi-breath patterns of recently reported FOSs and discuss their applicability in RR monitoring. Finally, we summarize the pros and cons of each category and point out the development directions of next-generation sensors.

2. The techniques used in FOSs for breath monitoring

FOSs have many sensing principles commonly used for RR monitoring, such as intensity-based, fiber grating and interferometer. Different sensing principles can be applied fulfil the different requirements in detection applications. Herein, we will introduce the structure and sensing mechanism of FOSs commonly used in RR measurement, and briefly analyze its advantages and disadvantages.

2.1. Intensity-based FOS

The early intensity-based FOSs are based on the displacement or bending of fibers, as shown in Fig. 2(a). In the classical setup, at least two fibers are placed in series. The light source and the detector are connected with the separated fiber ends [18]. Thus, the light intensity at the detection end alters as a consequence of the movement or displacement of fiber in different direction, including in lateral, longitudinal, angular, or differential directions.

Another type of intensity-based FOSs is basically the modulation of the light transmission in fiber, in which the bending of fiber induces the change of output light intensity. There are to forms of fiber bending, namely microbend (Fig. 2b) and macrobend (Fig. 2c). Microbend FOSs are suitable to measure the strain, pressure, force, position and acceleration, which mechanically coupled to the FOS and deforms the fiber [19]. In the microbend cases, the fiber is usually placed inside a teeth-like deformer, which contains upper and lower teethes. As the measurand is mechanically added on the deformer, the distance between the two layers of teeth is reduced and microbend along the fiber. There is typically a linear relationship between the continuous movement of the deformer and the output light intensity [20]. In the setup of macrobending, rather than the implication of deformer, the fiber itself is formed into a bending formation, e.g., U-shape, round loop(s), sinusoidal shape, etc. [21] Then the bended fiber is placed onto elastic elements for form a FOS. As the elastic element is deformed, the output light intensity will change as a result of the changes of fiber bending radius.

2.2. Fiber grating

Fiber grating is a diffraction grating with permanent period change of RI in the fiber core. From the perspective of the RI modulation period, it can be divided into short period fiber grating (period <1 μm) and long period fiber grating (LPG) (tens to hundreds of microns) [22]. Based on the direction of axial index modulation, short period grating can be divided into fiber Bragg grating (FBG) and tilted fiber Bragg grating (TFBG).

The FBG can be regarded as a narrow-band filter in fiber core, due to its coupling mechanism that it only reflects one wavelength and transmits all other wavelengths, as shown in Fig. 3a. The only reflected wavelength is the central wavelength (λ_B) of FBG, which is determined by.

$$\lambda_B = 2n_{eff}\Lambda \tag{1}$$

where n_{eff} is the effective refractive index (RI), Λ is the period of the FBG. The external perturbation on FBG (e.g., strain or temperature change) can result in a shift of central wavelength.

In TFBG, the grating was fabricated with a certain angle between the vector direction and the fiber axis direction. Thus, there are additional fundamental modes coupling into a series of backward cladding modes, as shown in Fig. 3(b). As the energy of cladding mode disappears rapidly, only the transmission peak of cladding mode is left in the

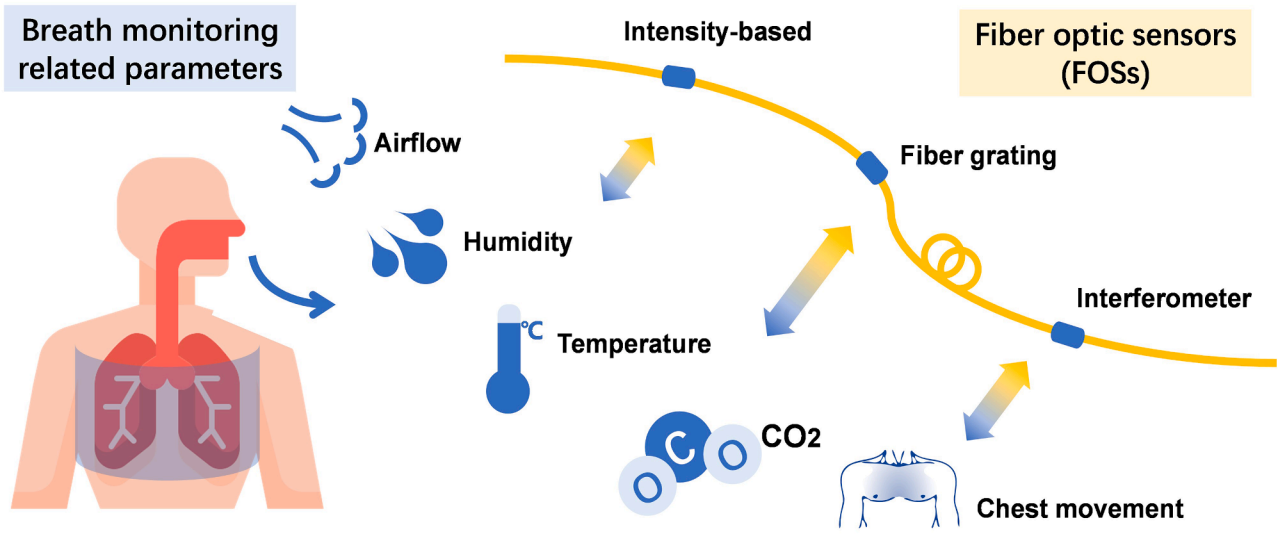

Fig. 1. Key techniques used in FOSs for RR monitoring via various breath related parameters.

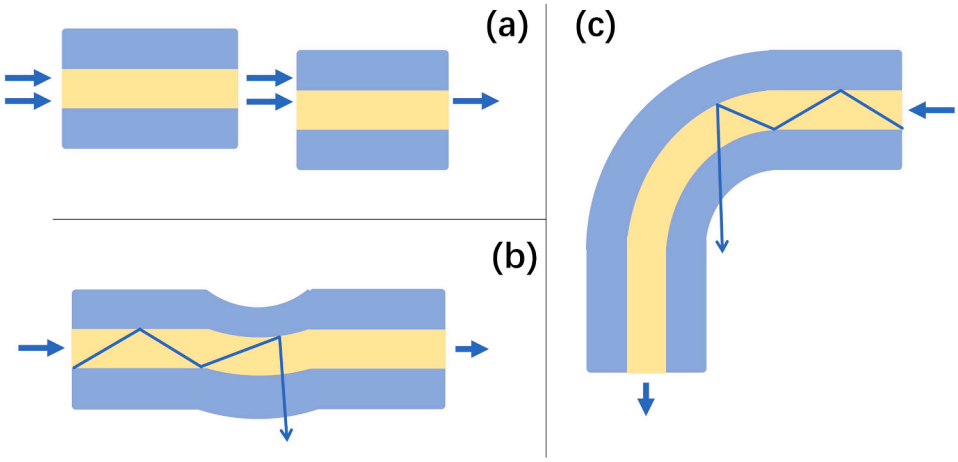

Fig. 2. Intensity-based mechanism of FOSs by detecting the fiber (a) displacement, (b) microbending and (c) macrobending.

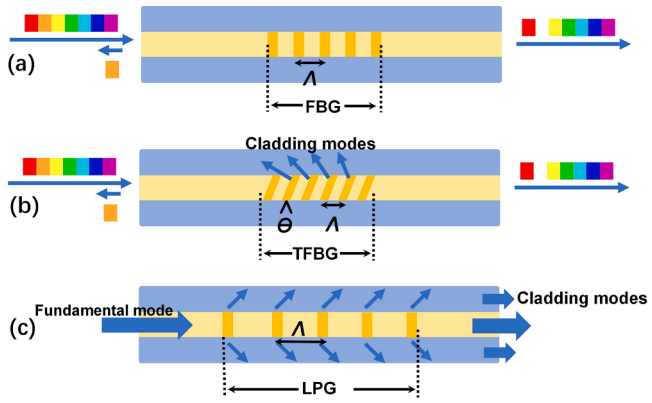

Fig. 3. Schematic diagram of structure and optical propagation of (a) FBG, (b) TFBG and (c) LPG.

grating spectrum. The coupling wavelength (n^i_{clad}) of each cladding mode can be expressed as.

$$\lambda^i_{clad} = \left(n_{core} + n^i_{clad}\right)\Lambda/\cos\theta \tag{2}$$

where n_{core} is the core effective RI, n^i_{clad} is the effective RI of the i-order cladding mode, θ is the angle between the directions of grating vector and the fiber axis, and Λ is the period of the TFBG. The cladding mode is sensitive to the changes of external RI. According to the phase matching condition, when the n^i_{clad} is close to the RI of surrounding environment, the maximum detection sensitivity can be achieved.

In the mode coupling of LPG, there is no backward reflection, but with coupling between the core fundamental mode and the multiple cladding modes in the same direction of light transmission, as shown in Fig. 3c. Thus, LPG can be regarded as a band stop filter. In LPG, there is a resonant mode coupling between core mode and cladding mode, which can occur at the wavelength determined by.

$$\lambda = \left(n_{core} - n^i_{clad}\right)\Lambda \tag{3}$$

where n_{core} is the core mode effective RI of LPG, n^i_{clad} is the effective RI of i-order cladding mode, and Λ is the period of the LPG. The resonance wavelength is a function of the difference between the effective RI of core mode and cladding mode. As the RI of cladding mode is sensitive to the change of external environment, the shift of resonance wavelength could be utilized as the indicator of change in external environment.

2.3. Interferometer

The principle of interferometer is the interference of two light beams with certain difference in optical paths. Basically, there are four types of interferometers, which are Mach-Zehnder, Fabry-Pérot, Michelson and Sagnac interferometers, in which the former two are widely used in the FOSs for RR monitoring according to the recent publications [20].

The structure of Mach-Zehnder interferometer (MZI) is shown in Fig. 4a, which consists of two 3 dB couplers and several sections of single-mode fiber (SMF). The input light is divided into two beams with the equal intensity through the first coupler and enter the reference and the sensing arms, respectively. In the second coupler, the two lights combine again. The difference in the optical paths of the two light beams can be induced by the two arms with different lengths. When the MZI works as a sensor, the reference arm is isolated from any external changes as much as possible, while the sensing arm experiences the measurands induced by the external changes. Both the length and RI of the sensing arm could be altered by the changes in external environment, resulting the change of the final interference signal.

Fabry-Pérot interferometer (FPI) is typically formed by two parallel reflecting surfaces with different reflectance of R_1 and R_2, and separated by a distance of L, as shown in Fig. 4b. Based on whether the reflecting surfaces are within the fiber or not, FPI can be classified as extrinsic and intrinsic types.

For extrinsic FPI, there is an air cavity between two fiber ends with a supporting structure. The extrinsic FPI could commonly achieve high finesse interference signals with highly reflecting surfaces. However, coupling efficiency is usually not high for this type of FPI. During fabrication, careful and precise alignment is required to form the interference cavity.

The intrinsic FPI contain reflecting surfaces within the fiber. There are various methods to fabricate intrinsic FPI, e. g., through micro-machining, using two FBGs in series, through chemical etching, by thin membrane deposition, using special fibers, or creating an air bubble in fibers [20]. When the cavity is formed by surfaces with low reflectivity, the intrinsic FPI can be simplified as a two-beam interferometer. The reflection spectrum is determined by the phase difference δ between the beams generated from the two reflections [20], that is.

$$\delta = 4\pi nL/\lambda \tag{4}$$

where, n, L and λ are the effective RI of the cavity medium, the physical length of the cavity, and the wavelength of incident light, respectively. The external perturbations, e. g., strain, temperature, humidity, etc., could change both the cavity length and effective RI of the intrinsic FPI, and eventually cause the shift of phase difference.

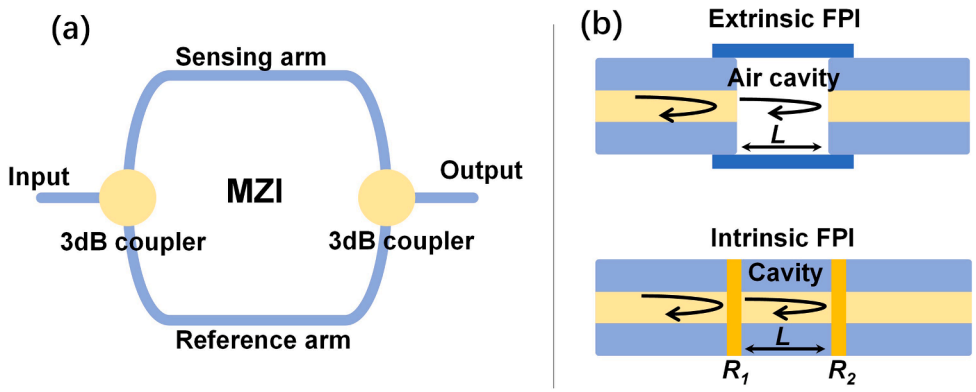

Fig. 4. Schematic diagram of (a) MZI and (b) FPI.

3. Foss for respiratory monitoring

In the following content, the recent reported breath FOSs will be classified according to the sensing principle, i.e., airflow, humidity, temperature, CO_2 concentration, and chest-wall-movement based. Selected demonstrations that highlight their potential or progress in RR monitoring will be reviewed and compared in terms of response/recovery times, packaging solution, and capability to measure multi-breath patterns, etc.

3.1. Respiratory airflow-based FOSs

At complete rest, the typical adult male exchanges approximately 0.5 L (0.4 L for female) of air per breath at a rate of 12 times per minute, resulting in a minute ventilation rate of about 6 L of air per minute [23]. In calm, at-rest breathing, the body generates a modest ±3 mmHg pressure swing to create inhalation and exhalation flow [23]. For the patients with lung disease, such as COPD, the averaged peak inspiratory flow is tested to be still higher than 30 L/min [24], which is significant enough for FOSs with typical sensitivity to detect. In some study, the minimum value of inspiratory peak flow was determined as 10 L/min [25], which is probably the required limit of detection (LOD) for the airflow based breath sensors. During physical exercise, the peak inspiratory flow could be as high as 414 mL/min [26]. Various types of the respiratory-airflow based FOSs have been reported mainly by utilizing the mechanisms of FPI, FBG, intensity-based, as summarized in Table 1.

An in-line fiber FPI micro-cavity was fabricated by unitizing the void in the silica fiber core generated by the catastrophic fuse effect. The resultant fiber containing single open void was cleaved and spliced to an SMF to form the in-line FPI based fiber spirometer, which converting the breath airflow into strain variations to the optical fiber, modulating the FPI spectral response [33]. Another kind of fiber FP sensor was developed based on the biaxially oriented polypropylene (BOPP) film. The FPI was form by the SMF end face and the BOPP film. The film changed its shape when exposed to the breath airflow, resulting in the change of FPI cavity length. Due to the low Young's modulus and thinner thickness of the BOPP film, the sensor demonstrated a high pressure sensitivity of −0.581 nm/Pa [27]. Recently, we have also reported a wearable breath sensor based on fiber-tip microcantilever, in which a micro FPI was formed between the microcantilever and the end-face of the fiber, as shown in Fig. 5. The cavity length of the micro FP interferometer was reduced as a result of the bending of the microcantilever induced by breath airflow. The breath sensor achieved a high sensitivity of 0.8 nm/(m/s) by detecting the reflection spectrum upon applied flow velocities from 0.53 to 5.31 m/s [31]. When mounted inside a wearable surgical mask, the sensor demonstrated the capability to detect various breath patterns, including normal, fast, random, and deep breaths.

More simplified methods have been demonstrated by utilizing the intensity-based techniques. The displacement of fiber itself under the breath airflow has been unutilized as sensing mechanism. In the design of plastic optical fiber (POF) pair, the two end faces of the POF were aligned to face each other. The force of the exhaled air caused the misalignment of the POF pair, resulting in the coupling loss [30]. A smartphone-based breath sensing system was developed using 3-POF multiplexing. The breath airflow-induced displacement of the fibers could alter the intensity contribution of each fiber in the output image [34]. A single mode–multi mode–single mode (SMS) fiber structure was also utilized as a breath sensor, in which the airflow induced bending of the multimode fiber (MMF) could change its RI distribution and result in the power variation of the output [32]. To enhance the sensitivity to mechanical perturbations, a liquid-filled photonic crystal fiber (PCF)-based sensor was developed to change the transmission properties of the waveguide, resulting in a sensitive carrier to weak vibrations, including the finger movement and human breathing [35].

FBG-based sensors have also been developed to sensing the breath airflow based on the temperature or (and) pressure effects. In one

Table 1
Comparison of various intensity-based FOSs for respiratory monitoring.

Principle	Key component	Packaging	Response /recovery time	Multiple breath pattern	Percentage error, # of subjects	Ref
Flow pressure induced	FPI	Medical respirator	NA	Yes	NA 2 subjects	[27]
Flow pressure effect and temperature difference	FBG	Nasal oxygen cannulas	NA	NA	Total relative error <5 %, 10	[28]
Airflow induced strain	FBG	V shaped rubber fixture over nose	NA	No	NA, 10	[29]
Airflow induced displacement	Two aligned POFs	Metallic ring	maximum sensitivity of 1.2 breaths/s	NA	NA, 1	[30]
Airflow induced -microbending	Fiber-tip microcantilever	Disposable surgical mask	0.3 s, 0.5 s	Yes	NA,1	[31]
Airflow induced -bending	SMS fiber	Thin plastic film in gas mask	NA	Yes	NA, 1	[32]

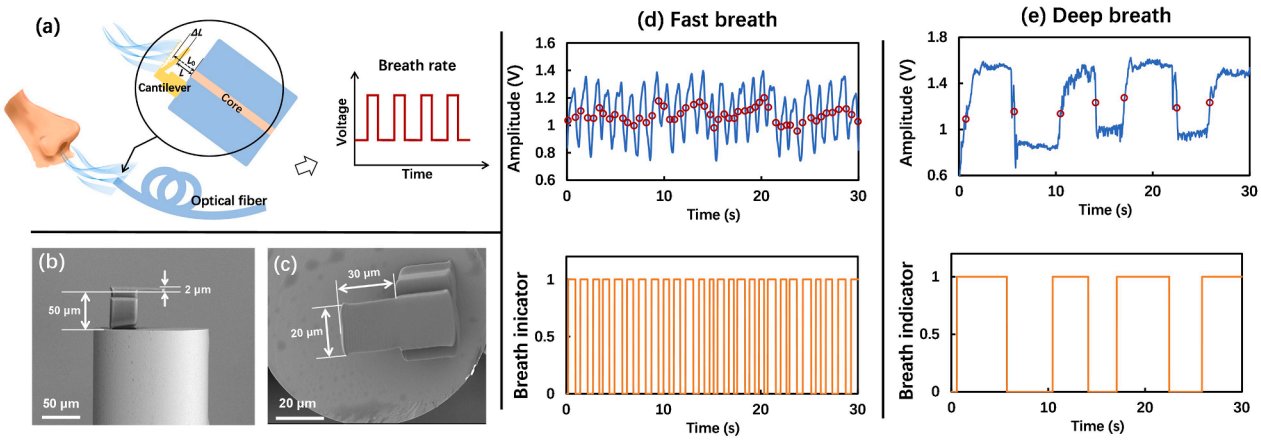

Fig. 5. (a) Schematic diagram of RR monitoring FOS based on fiber-tip microcantilever; (b) and (c) are the representative scanning electron microscopy (SEM) micrographs of fiber-tip microcantilever; (d) and (e) are recorded representative breath patterns of fast and deep breath with different RR. [31].

design, an optical fiber with a Bragg grating was mounted in a nasal oxygen cannula to monitor the respiratory activity by the cumulative effects from both temperature and pressure of exhaled air [28]. In another design, the FBG was bond over a cantilever which transducing the nasal airflow into strain variations [29].

The most significant advantage the respiratory airflow-based FOSs is probably the fast response (typical response time less than 1 s). For those relying on the external sensing elements, such as cantilever and membrane, the sensitivity and response time are usually limited by the sensitivity of these elements to breath airflow. Thus, a systematic study of the key parameters, e.g., the spring constant of cantilever, the Young's modulus and thinness of membrane, are highly recommended. For those based on the displacement or bending of the fiber itself, the breath sensing performance is easily impacted by the human movement. Thus, a proper packaging of the sensor is required to both amplify the pressure effect of airflow and minimize the side effects of ambient temperature and body motion.

3.2. Temperature based FOSs

The temperature of a healthy human being is about 37 ℃ while the exhaled breath temperature varies around 31–35 ℃ [36]. That means a difference of about 2–6 ℃ can be found between the air temperature from alveoli and the exhaled temperature. It was also reported that the temperature difference between inhaled and exhaled air can reach approximately as high as 15 ℃ [37]. Thus, several types of FOSs with the capability for reliable temperature measurement can be utilized to monitor human breath.

Shape memory photonic crystal fibers (SMPFs) was fabricated by coaxially growing Al_2O_3/ZnO photonic shells onto the polyester fiber surface. The pyroelectric effect of ZnO endows the SMPF's temperature-sensing capability, which can be used as a shape memory temperature sensor to sensitively detect mouth respiration (33 °C) and nose breathing (31 °C) even after deformation [38].

Temperature of exhaled air was also directly measured by FBG, resulting in its Bragg wavelength changes reflecting the breathing rate [39]. The temperature and pressure effects have been both unutilized for FBG-based breath sensing in [28]. Temperature sensing film of thermochromic pigment and epoxy mixture was fixed in front of a POF by a polymethyl methacrylate (PMMA) tube, which can change the color from white to red corresponding with the respiration process of exhalation and inhalation [40]. Such color change was then detected by measuring the intensity of the reflected light. The setup was tested to be fully compatible with magnetic resonance imaging (MRI) system without deteriorating the MR image.

Though FOSs, especially the FBG-based types, demonstrate the sensitive and linear responses, there is not too many reports of the ones based on the temperature difference between the inhaled and exhaled air. This was probably due to the issue of cross sensitivity, e.g., between temperature and strain, or between humidity and temperature. Besides, the impact of the ambient temperature, especially in out-door environment, is also a critical issue for the FOSs to achieve a reliable sensing performance. On the other hand, some of the selected reports have utilized the cross sensitivity to achieve multi-vital parameter measurements simultaneously, by applying additional signal processing solution [41–49].

3.3. Humidity based FOSs

The inhaled and exhaled air differ in the content of water vapor. Inhaled air is at environmental conditions (relative humidity (RH) from 40 % to 80 %), while the exhaled air is at body temperature and saturated by vapor (RH = 100 %) [50]. Therefore, various types of FOSs have been reported to measure the RR from the difference of water vapor contents between inhaled and exhaled air. There are two types of humidity-based breath FOSs, according to whether including a hygroscopic material as the sensing element or not.

One type of the humidity-based breath FOSs is based on the change in volume (physical thickness) and RI of the hygroscopic material as they are exposed to changes of surrounding RH, as summarized in Table 2. Hence, the performance of the sensors is strongly dependent on the properties of these hygroscopic materials [51]. The fabrication process is typically more complicated. In addition, their life time may also become an issue induced by the material alteration or loose combination due to temperature change or chemical corrosion [52]. Limited by the diffusion coefficient of water molecule into the hygroscopic material, the response and recover times are typically in the order of second (even longer than 100 s) for those FOSs using conventional material such as, polyvinyl alcohol (PVA), agar, agarose, etc. By applying nanomaterials, especially-two-dimensional nanomaterials such as graphene oxide (GO), the response and recover times could be reduced to tens of microseconds.

A surface-plasmon-resonance (SPR) based fiber device was fabricated by using a PVA film and gold coating on the flat surface of a side-polished POF [61]. The high humidity of the breath could change the thickness and RI of the PVA coating, and thus alter the resonant wavelength. The response and recovery times were determined to be 0.44 s and 0.86 s, respectively. This sensor suffers from the temperature cross-sensitivity. Humidity detection based SPR breath sensor was also developed on twisted LPG coated with WS_2 film [62]. The times of respiratory rise and fall were 0.315 s and 1.465 s, respectively.

A plasmonic fiber tip for RH detection by integrating a gold

Table 2
Comparison of various humidity-based FOSs with hygroscopic materials for respiratory monitoring.

Principle	Key component	Packaging	Response /recovery time	Multiple breath pattern	Percentage error, # of subjects	Ref
Humidity-based (PAH/SiO2 NPs)	Fiber tip multilayer of PAH/SiO2 NPs + FBG nearby	Oxygen mask, nasal cannula, non-rebreathe mask	NA	Yes	Highest mean accuracy of 88.1 %, 15	[53]
Humidity-based (agar)	FBG	Homemade fittings under the nose	44.4 s, 111.7 s	Yes	Mean percentage errors $\leq$ 2.29 %, 6	[54]
Humidity-based (GO)	U-shape PPMF based interferometer coated with GO film	NA	0.28 s	No	NA,1	[55]
Humidity-based (gelatin)	Microknot resonator superimposed on MZI	Breathing mask	0.084 s, 0.029 s	Yes	NA, 1	[21]
Humidity-based (chitosan)	Suspended tri-core fiber based FPI	A solid substrate with an adhesive polyimide tape	0.08 s, 0.07 s	No	NA, 1	[51]
Humidity-based (GO)	GO on TFG	NA	0.042 s, 0.115 s	Yes	NA,1	[56]
Humidity-based (agar)	FBG coated with agar	Inside a needle within the ducts connecting the ventilator	90 s	Yes	~2%, NA	[57,58]
Humidity-based (SnO_2)	SnO_2 on a four-bridge MOF	NA	0.37 s, 0.38 s	No	NA,1	[59]
Humidity-based (polyimide)	FBG–FPI	NA	0.4 s, 5 s	No	NA,1	[44]
Humidity-based (MoS_2)	MoS_2 nanosheets coated SPF	NA	0.85 s, 0.85 s	No	NA,1	[60]

nanomembrane onto the end-face of a MOF, with response and recovery times of 156 ms and 277 ms, respectively, to detect the different breath patterns [63]. Another humidity based sensor was based on the FPI of the fiber tip multilayer film made of hygroscopic material PAH/SiO2 nanoparticles, together with the FBG located near [53]. Every breath causes a shift in the wavelength reflected from the FBG and intensity change in the overall reflection spectrum. Various types of packaging have been designed and evaluated, such as using oxygen mask, nasal cannula and non-rebreathe mask, etc. Another similar FBG-FPI probe for breath sensing has been fabricated based on a layer of thin polyimide (PI) film on the end face of SMF [44]. The cascaded FBG was used for temperature calibration and elimination of the temperature cross-sensitivity in breath sensing with response time of 400 ms and recovery time of 5 s.

FBG was functionalized by using 1 wt% agar which was sensitive to the surrounding humidity [54]. The sensor has been tested to be with low breath detection error of 2.29 % in a study of 6 subjects, however with a quite long response and recovery times of 44.4 s and 111.7 s, respectively. Another FBG breath sensor coated by agar was housed in a needle allowing an easy insertion of the probe within the ducts connecting the ventilator to the patient, with a detection error of 2 % [57]. The response is similarly as long as 90 s. The FBG-based needle also has been applied to simultaneously measure the RH and BR during mechanical ventilation [58].

U-shape panda polarization-maintaining fiber (PPMF) based microfiber interferometer was coated with GO film, which has a strong ability to absorb water vapor [55]. The sensor consists of a microknot resonator superimposed on a MZI produced by a tapered SMF, with gelatin film

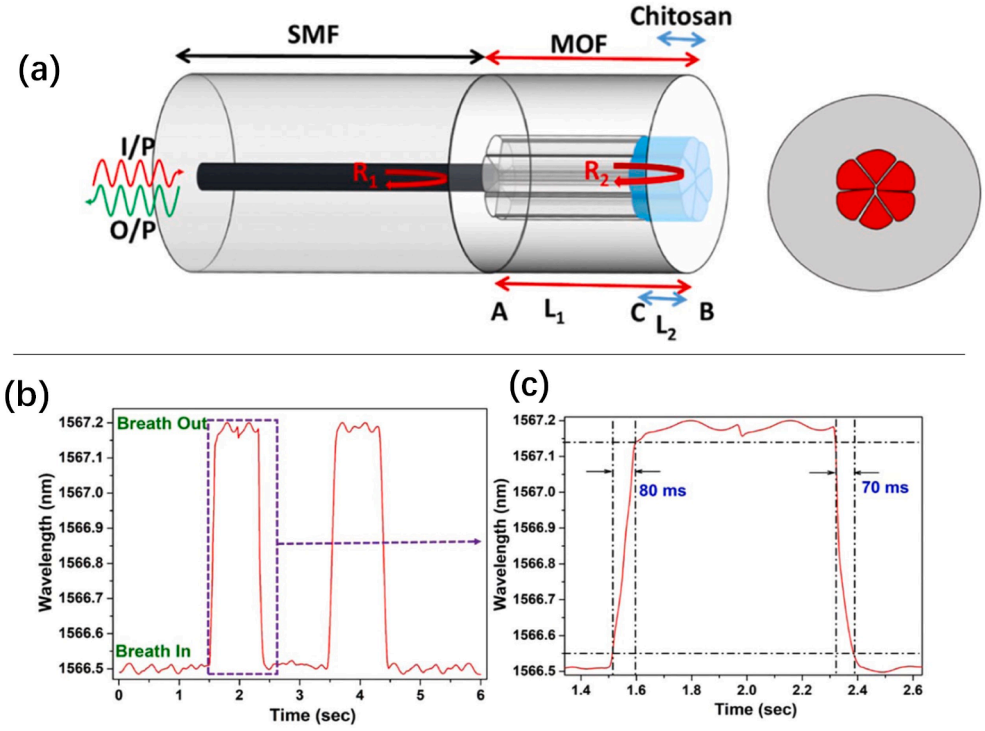

Fig. 6. (a) Schematic illustration of the humidity-based breath FOS based on a suspended tri-core MOF using a FPI configuration, and the cross section of the fiber; (b) and (c) are the recorded human breath cycle. [51].

deposited on the surface of the MZ arm [21]. The infiltration of water molecules on the gelatin film decreased its RI, resulting in the variation of transmission intensity. The sensor has a fast response (84 ms) and recovery time (29 ms), and a large dynamic transmission range.

A low-finesse FPI sensing head was formed for breath sensing using SnO_2 sputtering deposition on a four-bridge microstructure optical fiber (MOF) [59]. Due to the physisorption phenomena of the interaction between SnO_2 and H_2O molecules, the output optical spectrum changed as the exhaled air arrived to the SnO_2 nanomembrane. The sensor presented a response time of 370 ms and a recovery time of 380 ms. A chitosan polymer filled suspended tri-core fiber as a FPI for breath monitoring unitizing the chitosan polymer to execute RH sensing [51], as shown in Fig. 6. Both the RI and volume of polymer changed after water adsorption, resulting in the shift in the wavelength as well as the power of the reflected light. The probe shows a fast response during human breath monitoring with a rising time and recovery time of 80 ms and 70 ms, respectively.

The largely tilted grating planes of the TFG can induce a set of polarization-dependent cladding modes and strong evanescent field to couple with the humidity dependent dielectric of GO layer [56]. Since the human breathing contains much water vapors, the wavelength shift of the resonant dip will lead to the power decrease of transmission. A thin film made of alternating polyethylenimine (PEI) and GO layers was selected as sensitive coating. It was deposited on a SnO_2-sputtered fiber core in a dip-assisted layer-by-layer assembly [64].

In an agarose coated macro-bend fiber (AC-MBF) sensor, stronger resonance dips was found at 2 μm region, which is at the peak of water absorption better for humidity sensing [65]. For breath testing, AC-MBF sensor is with fast response time and recovery time of ~300 ms and 600 ms, respectively. MoS_2 nanosheets coated on sidepolished optical fiber (SPF) for the enhancement of humidity sensing as the MoS_2 nanosheets possess exceedingly high surface/volume ratio [60]. When the breath air arrived the sensor surface, charges will be transferred from H_2O to MoS_2 which induce the change for the effective RI of the deposited MoS_2 nanosheets and eventually cause the change of optical transmitted power.

The other type of breath FOSs is free of hygroscopic materials, as summarized in Table 3, which allowing them to be fast-response, low-cost, with long lifetime and robust. The sensing mechanism is usually based on the RI change induced by the water vapor in the exhaled air or the condensed water film on the sensing surface.

A miniaturized cross-axial open-cavity FPI was formed by a 45°-angled side-hole fiber fabricated by a simple end-face polishing process [66]. The sensor was packaged into a polypropylene tube. When the humidity inside the tube increased due to the exhaled air, the water vapor concentration of the in-fiber microchannel will alter optical properties of the open cavity. The response time was typically around 460 ms since it took time for the inter-diffusion of water vapor between the open cavity and the external environment.

A breath sensor was directly constructed by sandwiching a segment of hollow core Bragg fiber (HCBF) between two SMFs [52]. When the breath reached the HCBF-based sensor, moisture of exhaled air condensed on the outer surface to form an uneven water film, which will destroy the uniform silica reflecting surface and increase the transmission loss at the guided band. The sensor presented a rapid response time of ~0.15 s and recovery time of ~0.65 s. The sensor was turned out to be insensitive to the variation of temperature and curvature, however sensitive to the distance between the human face and the sensor due to the lack in well-designed packaging.

A high-sensitive optical fiber humidity sensor based on in-line Michelson interferometer (MI) was proposed and demonstrated. The MI was formed by an asymmetric dual-core fiber (DCF) spliced with a short section of MMF. The MMF served as fiber coupler, while the DCF created a strong intermodal interference to strengthen the interaction between light and ambient moisture [67]. The response and recovery times were 562 ms and 308 ms, respectively. Another humidity sensor was fabricated by sandwiching a taper between PCF and a SMF. The taper and collapsed region in PCF excite high-order modes and couple them with core mode to form a MI [71]. Both the humidity-induced RI change in the air holes of PCF and on the region of fiber taper could alter the high-order modes and thus detect the breath signal. The sensor was tested to be with a rise/recovery time of 400/200 ms. A breath sensor is based on an integrated MZI consisting of two off-axis twisted deformation points and an air channel passing through the core of a SMF [70]. The high-humidity air in the channel determined the RI and eventually affected the optical path difference of the MZI, resulting in the shifts in the resonance wavelength.

In a hybrid-structured microtip FPI sensor, a UV cured polymer film was deposited on the end facet of a SMF and a microtip was fabricated on top of the polymer film, forming a ultracompact fiber-tip FPI [68]. The sensing mechanism is based on the increase of microtip effective length after it swelled because of the diffusion of water vapor molecules. Though the increase of water molecules may also reduce the RI of the microtip, the overall output of the sensor presented a redshift of the reflection spectra. The response and recovery times of the hybrid microtip FPI sensor for human breathing were 0.65 s and 0.6 s, respectively,

An eccentric FBG was inscribed in a SMF to excite a stable core mode and sensitive cladding modes, as shown in Fig. 7 [69]. The interface evanescent field of the cladding mode was highly sensitive to the humidity-induced RI variation, while the stable core mode could be used a self-compensation. It was with fast response (92 ms) and recovery times (100 ms). Different breathing patterns can be recognized.

Table 3
Comparison of various humidity-based FOSs without hygroscopic materials for respiratory monitoring.

Principle	Key component	Packaging	Response /recovery time	Multiple breath pattern	Percentage error, # of subjects	Ref
Humidity-based	45 angled side-hole fiber-based FPI	Polypropylene tube	0.46 s	No	NA,1	[66]
Moisture condenses on sensor surface	HCBF	NA	0.15 s, 0.65 s	No	NA,1	[52]
Humidity-based SPR	PVA film and gold coating on the surface of a side polished POF	NA	0.44 s, 0.86 s	No	NA,1	[61]
Humidity-based SPR	Twisted LPG coated with WS_2 film	NA	0.315 s, 1.465 s	No	NA,1	[62]
Humidity-based	In-line MI based on DCF and MMF	NA	0.562 s, 0.308 s	No	NA, 1	[67]
Humidity-based	Hybrid-structured microtip FPI	NA	0.65 s, 0.6 s	No	NA,1	[68]
Humidity-based RI change	Eccentric FBG	Breathing tube	0.092 s, 0.1 s	Yes	NA, 1	[69]
Water condensation on the sensing membrane	integrating a gold nanomembrane onto the end-face of an MOF	NA	0.156 s, 0.277 s	Yes	NA,1	[63]
Humidity-based RI change	MZI and air channel through the core of a SMF	NA	0.125 s, 68 s	No	NA,1	[70]

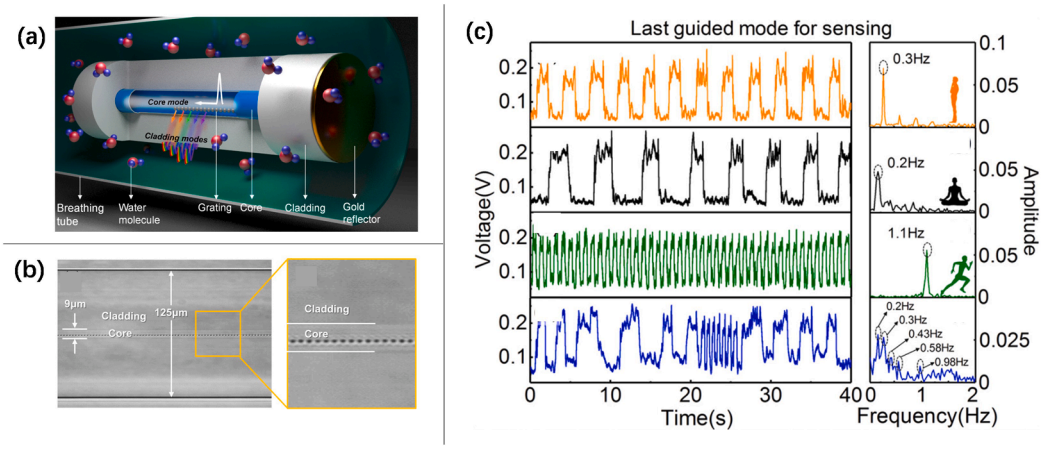

Fig. 7. (a) Schematic configuration of the EFBG; (b) Side-view micrograph of the EFBG; (c) The responses of last guided mode to different breathing patterns and their corresponding fast Fourier transforms (FFT) results: normal, slow, fast, random breath (from top to bottom). [69].

3.4. Carbon dioxide (CO_2) concentration-based FOSs

During inhalation, the fresh oxygenated air flows into branching progressively smaller airways to ultimately inflate the alveoli and exchange O_2 for CO_2. CO_2 is expelled upon exhalation and the cycle begins anew. Humans do not absorb all of the inhaled O_2 for metabolism; inhaled air contains 21 % O_2 while exhaled breath contains approximately 16 % O_2 and 5 % CO_2 [23]. Thus, ideally based on the difference of CO_2 in inhaled and exhaled air, the RR can be determined by CO_2 FOSs.

In CO_2 FOSs, the key sensing element is CO_2 sensitive material. It can shrink or dilate as the response of change in CO_2 concentration. Then its change on RI, volume, or mechanical constraint on the fiber could be detected by FOSs. Several selected reports have demonstrated the feasibility of using FOSs to measure the CO_2 concentration in breath. However, recently there is seldom work reporting using the CO_2 FOSs to measure the RR, probably limited by the long response time of the sensors that comparable to the time of single human respiration.

Polyimide-coated FBGs for CO_2 detection based on the mechanism of CO_2-induced volume dilation in the polyimide matrix, which resulted in a shift of the Bragg wavelength [72]. The detection results indicate that the polyimide-coated FBGs were of good reversibility and repeatability within CO_2-N_2 cycles. A LPG based CO_2 sensor was coated with HKUST-1, a material from the metal organic framework family [73].

The CO_2 sensitive dye ion-pair (thymol blue and tetramethylammonium hydroxide) were encapsulated inside organically modified silica forming an extrinsic FPI cavity for the simultaneous measurement of CO_2 and RH, as a combination of colorimetric measurement and FPI [45]. The applicability of the sensor was demonstrated by measuring the CO_2 and RH exhaled from human breath with a percent error of 3.1 % and 2.2 % respectively. With the similar mechanism, dyes of thymol blue and tetraphenylporphyrin tetrasulfonic acid hydrate (TPPS) were coated on the distal ends of a 2 × 2 optical fiber coupler for simultaneous measurements of NH_3 and CO_2 in breath [74]. With the FPI based methodology, other types of CO_2 sensing layer, such as polyhexamethylene biguanide (PHMB), has also been utilized for breath CO_2 sensing [75].

Recently, it has been developed a small gas cell attached to the distal end of a thin optical fiber probe, that could be inserted into airways via a catheter or a bronchoscope [76]. The target gas penetrates the cell through small holes. A polyvinylidene chloride film is attached to the distal end of the hollow optical fiber. The measurement of the CO_2 was then obtained with Fourier-transform infrared spectroscopy. Measurement error of the mentioned system was ± 0.3 %, minimum threshold of 0.45 % of CO_2.

3.5. Chest-wall-movement based FOSs

Breathing is made possible by the work of the respiratory muscles, with the diaphragm and external intercostal muscles playing a major role during inspiration. The diaphragm contracts itself and moves downward producing a pressure difference causing air to enter the lungs [16]. The contraction of the intercostal muscles causes the ribs to elevate which results in the expansion of the chest cavity allowing a greater volume of air to enter. This amount of air within the lungs causes an expansion of the chest wall diameter up to ~7 cm [77], with the cascade movements of abdomen and back. Basically, the breath FOSs that transform the cyclic expansion and contraction of the chest into a signal of RR is based on the strain measurement techniques. Thus, various types of FOSs that are sensitive to external strain change, including intensity based, FBG and interferometer, have been developed to measure the RR signal (Table 4).

FBG sensor is a competitive method for monitoring of respiratory behavior for chest [42,48] and abdomen [81,82] regions since the sensors are able to convert physical movement into wavelength shift, which is usually integrated into elastic belts for detecting breathing activities [83]. Two FBG sensors were encapsulated into a flexible matrix for monitoring both neck movements and respiratory activity, based on the movement induced strain on the FBG [46]. Both quite breathing and tachypnea have been detected by the proposed dual-sensor system. A polyimide-coated FBG sensor was encapsulated into a dumbbell shaped-flexible matrix to detect the movement of rib cage during breath [79]. The RR of the 10 volunteers undertaking 14 different working tasks was measured with an average error less than 5 %. A stretchable FOS based on an Ω-shaped optical fiber with two FBGs on the two ends, measuring the human skin-induced strain based on light intensity loss which can be featured by the reflected spectrum intensity variety of FBG [84]. It has been demonstrated to monitor human activities and physiological parameters, such as RR, joint bending/full-body movement, and muscle tension by mounted or worn on the body, as shown in Fig. 8a.

Based on the optical power attenuation created by the fiber bending during the breathing, various microbend-based FOSs have been developed using different types of optical fibers, including POF [85–87], hetero-core optical fiber [43]. A light-intensity modulation-based sensor utilizing the microbending effect in MOFs mounted inside a teeth-like structure was achieved, to detecting sleep apnea according to the RR signals that induced by the movements of human back when lying on the bed [88]. Similarly, a dual-path microbend fiber optic sensor was fabricated by clamping two separate layers of graded MOF between three layers of hole-mesh [89], as shown in Fig. 8b. When lying on the bed integrated with the sensor, the human body movements and vibrations, like heartbeats and respiration-caused vibrations, can cause

Table 4
Comparison of strain-based FOSs for respiratory monitoring.

Principle	Key component	Packaging	Response /recovery time	Multiple breath pattern	Percentage error, # of subjects	Ref
Abdomen movement-based	D-shaped SMF	Belt	NA	Yes	NA, 1	[78]
Rib cage movement	PI-coated FBG	Dumbbell shaped-flexible matrix	NA	Yes	Lower than 5 %, 10	[79]
Abdomen movement-based	SMS fiber	Belt	NA	No	An average Pearson Correlation Coefficient of 0.88, 6	[80]

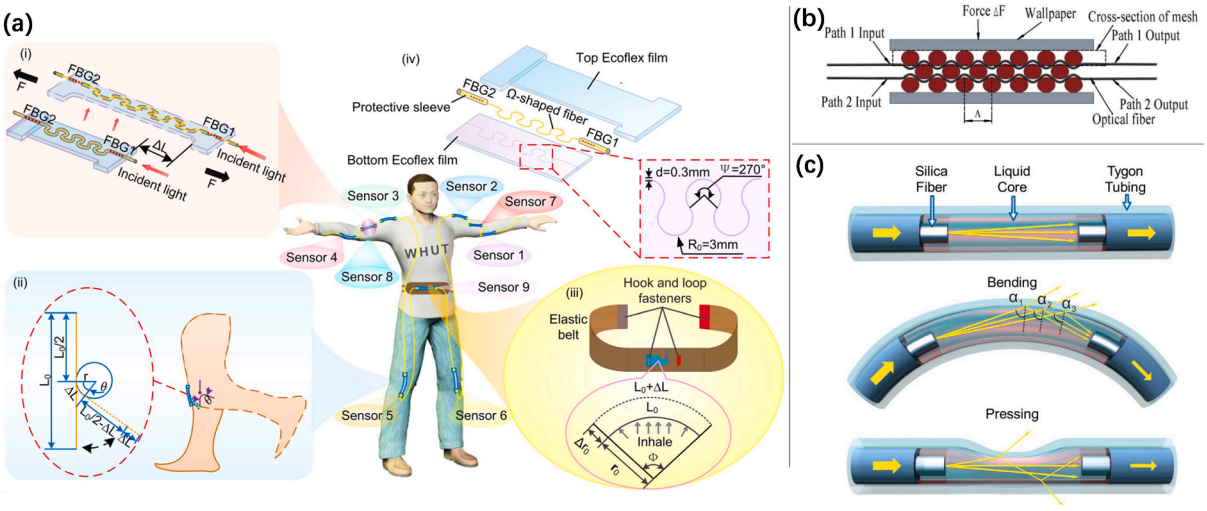

Fig. 8. (a) Working principle of the SSOF sensor [84]. Diverse human activities signals can be detected by the SSOF sensors after proper calibration. Schematic diagram of (i) Muscle tension monitoring, (ii) Joint bending angle monitoring, and (iii) Respiratory rate monitoring based on the SSOF sensor. (iv) 3D map of the SSOF sensor. (b) Cross-section pattern of dual-path microbend FOS [89]. (c) Schematics of the propagation of light in a straight, bent and pressed FLFFA [90].

fluctuations of the spectra of the microbend fiber sensor. In addition, a D-shaped SMF curvature sensor was encapsulated by poly-dimethylsiloxane (PDMS) and implanted into the belt to monitor RR under quiet and walking conditions [78].

By splicing a TCF between two SMFs, a TCF-based sensor was proposed for non-invasive vital sign monitoring, including respiration and heartbeat [91]. Similar with [35], a flexible liquid-filled fiber adapter (FLFFA) composed of a soft liquid-filled polymer tubing and two silica optical fibers was presented, as shown in Fig. 8c. It can be attached to a human body for versatile sensing applications based on the deformation of the tubing through bending or pressing [90]. When it attached to a volunteer's chest, the difference between normal breath and deep breath was obtained by analyzing the amplitude and the frequency of the respiration waveform diagram. A SMS fiber sensor was fastened by an elastic belt on the abdomen of a person will acquire the respiration signal when the person breaths, which will introduce front and back movement of the abdomen, and thus bend of SMS fiber structure [80]. In the test of 6 volunteers, an average Pearson Correlation Coefficient of 0.88 of the respiration signals has been achieved, which agreed very well with that of commercial belt respiration sensor.

An in-line few-mode fiber MZI (FMF-MZI) sensor was proposed to measure the RR and respiration volume by sensing the bending of the FMF attached to the abdomen [92]. Similarly, an FBG-based MZI system has been developed for respiration, pulse wave and heart sound [47]. Another fiber optic MZI based smart mattress constructed by sandwiching SMF with two PVC layers was fabricated. It has been applied to measure the RR and HR by detecting the pressure induced the axial strain on fiber [93]. In another work, by splicing a segment of seven-core fiber (SCF) on both ends of SMF and tapering it into dual biconical SCF, a SCF-based MZI sensor was formed to vibrations applied on the interferometer induced by rib cage movement [41].

As a strain measurement solution, the chest-wall-movement based FOSs are typically either adhered on the body surface directly [84] or integrated into belts which worn by the subjects [78]. In other cases, the FOSs were encapsulated into flexible matrixes that inside the mattress [41,80,89] and seat back [94], or adhered on the *T*-shirt [79,95]. It is worthwhile to adjust the tradeoff between the detection sensitivity and the comfort of subjects. As directly mechanical strain-based methods, the FOSs' response is usually fast, however involving other vital parameters such as heart rate, body movement and pulse wave. Recently, some selected FOSs usually were demonstrated with the capability to measure multiple vital parameters simultaneously either by additional signal process algorithm [47,91] or the arrangement of multiple sensors [79].

4. Conclusions

In summary, we have reviewed fiber-based breath sensors with comprehensive investigation and detailed discussion. The significances of breath monitoring as a useful way to access the health condition were introduced in the application fields of clinical use, monitoring of work health and safety, analysis of physical exercise. Several key techniques of FOSs for measuring RR have been described, e.g., intensity-based, fiber grating and interferometer. We classified the recent reported FOSs according to the sensing principle (i.e., airflow, humidity, temperature, CO_2 concentration, and chest-wall-movement based) and then critically analyzed the advantages and disadvantages between them by reviewing the representative recent works. The performances of the FOSs were compared in terms of several key performance metrics (response time, capability to measure various breath patterns, accuracy, accessible package, etc.). Though considerable headway has been made in terms of the novel sensor design, improvement of response time, and

demonstration of measuring multiple vital parameters with high accuracy, some fields are still worth exploring.

A grand challenge is the feasibility of the developed FOSs into real applications. Much research in recent years has focused on elaborating the sensor design by introducing new sensing material and deliberate structure. This could enhance the performance of FOSs especially in terms of sensitivity. However, the breath induced vital parameters are usually not weak signal indeed. More efforts are suggested to be contributed to demonstrate the long-term stability, robustness in various environments, and the accuracy in a larger number of subjects.

Simultaneous measurement of multiple vital parameters is consistently attractive in the development of FOSs. A low-cost and efficient solution is to unitize the intrinsic cross sensitivity of FOSs to simultaneously measure various measurands (e.g., humidity and temperature, temperature and strain, etc.), if the demodulation of multiple parameters can be achieved by signal process algorithm without additional hardware cost. Another solution is to use multi-sensor design or develop hybrid FOSs, which could probably increase the complexity of the FOS system.

Wearability is another crucial performance metric of FOSs. To monitoring the RR, FOSs have been encapsuled into worn fabrics, mattress, chair, sit back, elastic belt, Oxygen tube, breath mask, etc. Indeed, the FOS itself is highly wearable due to the flexibility of fiber. However, the benchtop instruments (e.g., light source, spectrometer, photodetector, etc.) limit the feasibility of portable RR monitoring. More miniaturized demodulation system and package are favorable for wearable and portable RR monitoring using FOSs. Besides, as Covid-19 is continuing to spread around the world, there is a potential and opportunity for the wearable breath FOSs offer remote monitoring and management of patients, or even provide a new generation of early detection solution. We believe these challenges and opportunities for developing breath FOSs need more interdisciplinary collaborations to push this thriving field forward.

The remaining authors declare that they have no known competing financial interests or personal relationships that could have appeared to influence the work reported in this paper.

Declaration of Competing Interest

The authors declare the following financial interests/personal relationships which may be considered as potential competing interests:

Acknowledgement

This study was funded by the National Natural Science Foundation of China (NSFC) (62122057 and 62075136); Natural Science Foundation of Guangdong Province (2018B030306003 and 2020A0505100066); and the Science and Technology Innovation Commission of Shenzhen (RCYX20200714114524139 and JCYJ20200109114001806).

References

[1] C. Massaroni, A. Nicolò, D. Lo Presti, M. Sacchetti, S. Silvestri, E. Schena, Contact-based methods for measuring respiratory rate, Sensors 19 (2019) 908.
[2] M.A. Cretikos, R. Bellomo, K. Hillman, J. Chen, S. Finfer, A. Flabouris, Respiratory rate: the neglected vital sign, Med. J. Aust. 188 (2008) 657–659.
[3] A. Nicolò, C. Massaroni, L. Passfield, Respiratory frequency during exercise: the neglected physiological measure, *Front. Physiol.* 8 (2017).
[4] I. Smith, J. Mackay, N. Fahrid, D. Krucheck, Respiratory rate measurement: a comparison of methods, Br. J. Healthcare Assistants 5 (2011) 18–23.
[5] P. Barthel, R. Wensel, A. Bauer, A. Müller, P. Wolf, K. Ulm, et al., Respiratory rate predicts outcome after acute myocardial infarction: a prospective cohort study, Eur. Heart J. 34 (2013) 1644–1650.
[6] E. Helfenbein, R. Firoozabadi, S. Chien, E. Carlson, S. Babaeizadeh, Development of three methods for extracting respiration from the surface ECG: A review, J. Electrocardiol. 47 (2014) 819–825.
[7] K. Gupta, A. Prasad, M. Nagappa, J. Wong, L. Abrahamyan, F.F. Chung, Risk factors for opioid-induced respiratory depression and failure to rescue: a review, *Curr. Opin. Anesthesiol.* 31 (2018).
[8] T. Rantonen, J. Jalonen, J. Grönlund, K. Antila, D. Southall, I. Välimäki, Increased amplitude modulation of continuous respiration precedes sudden infant death syndrome: –Detection by spectral estimation of respirogram, Early Human Dev. 53 (1998) 53–63.
[9] P.B. Lovett, J.M. Buchwald, K. Stürmann, P. Bijur, The vexatious vital: neither clinical measurements by nurses nor an electronic monitor provides accurate measurements of respiratory rate in triage, Ann. Emerg. Med. 45 (2005) 68–76.
[10] P. Marcel-Millet, G. Ravier, S. Grospretre, P. Gimenez, S. Freidig, A. Groslambert, Physiological responses and parasympathetic reactivation in rescue interventions: the effect of the breathing apparatus, Scand. J. Med. Sci. Sports 28 (2018) 2710–2722.
[11] M. Grassmann, E. Vlemincx, A. von Leupoldt, J.M. Mittelstädt, O. Van den Bergh, Respiratory changes in response to cognitive load: a systematic review, Neural Plasticity 2016 (2016) 8146809.
[12] M. Grassmann, E. Vlemincx, A. von Leupoldt, O. Van den Bergh, The role of respiratory measures to assess mental load in pilot selection, Ergonomics 59 (2016) 745–753.
[13] B. Carballo-Leyenda, J.G. Villa, J. López-Satué, P.S. Collado, J.A. Rodríguez-Marroyo, Fractional contribution of wildland firefighters' personal protective equipment on physiological strain, *Front. Physiol.* 9 (2018).
[14] L. Puente-Maestu, J.G. de Pedro, Y. Martínez-Abad, J.M.R. de Oña, D. Llorente, J. M. Cubillo, Dyspnea, ventilatory pattern, and changes in dynamic hyperinflation related to the intensity of constant work rate exercise in COPD, Chest 128 (2005) 651–656.
[15] P. Gagnon, J.S. Bussières, F. Ribeiro, S.L. Gagnon, D. Saey, N. Gagné, et al., Influences of spinal anesthesia on exercise tolerance in patients with chronic obstructive pulmonary disease, Am. J. Respir. Crit. Care Med. 186 (2012) 606–615.
[16] C. Perezcampos Mayoral, J. Gutiérrez Gutiérrez, J.L. Cano Pérez, M. Vargas Treviño, I.B. Gallegos Velasco, P.A. Hernández Cruz, et al., Fiber optic sensors for vital signs monitoring. A review of its practicality in the health field, Biosensors 11 (2021) 58.
[17] P. Samartkit, S. Pullteap, Fiber Optic Sensor Applications for Vital Signs Monitoring: A Review, in: In *2019 7th International Electrical EngIneerIng Congress (iEECON)*, 2019, pp. 1–4.
[18] M. Anwar Zawawi, S. O'Keffe, E. Lewis, Intensity-modulated fiber optic sensor for health monitoring applications: a comparative review, Sensor Review 33 (2013) 57–67.
[19] L. Xuejin, D. Yuanlong, Y. Yongqin, W. Xinyi, L. Jingxian, Microbending optical fiber sensors and their applications, in: in *Proceedings of the 2008 International Conference on Advanced Infocomm Technology*, 2008, pp. 1–4.
[20] W. Lyu, S. Chen, F. Tan, C. Yu, Vital signs monitoring based on interferometric fiber optic sensors, Photonics 9 (2022) 50.
[21] Y. Yi, Y. Jiang, H. Zhao, G. Brambilla, Y. Fan, P. Wang, High-performance ultrafast humidity sensor based on Microknot resonator-assisted Mach-Zehnder for monitoring human breath, ACS Sensors 5 (2020) 3404–3410.
[22] K.O. Hill, G. Meltz, Fiber Bragg grating technology fundamentals and overview, J. Lightwave Technol. 15 (1997) 1263–1276.
[23] J.D. Pleil, M. Ariel Geer Wallace, M.D. Davis, C.M. Matty, The physics of human breathing: flow, timing, volume, and pressure parameters for normal, on-demand, and ventilator respiration, J. Breath Res. 15 (2021), 042002.
[24] M. Anderson, K. Collison, M.B. Drummond, M. Hamilton, R. Jain, N. Martin, et al., Peak inspiratory flow rate in COPD: an analysis of clinical trial and real-world data, Int. J. Chronic Obstructive Pulmonary Dis. 16 (2021) 933–943.
[25] M. Rahimi-Gorji, O. Pourmehran, M. Gorji-Bandpy, T.B. Gorji, CFD simulation of airflow behavior and particle transport and deposition in different breathing conditions through the realistic model of human airways, J. Mol. Liq. 209 (2015) 121–133.
[26] I. HOLMÉR, K. Kuklane, C. Gao, Minute volumes and inspiratory flow rates during exhaustive treadmill walking using respirators, Ann. Occup. Hygiene 51 (2007) 327–335.
[27] Y. Li, B. Dong, E. Chen, X. Wang, Y. Zhao, W. Zhao, et al., Breathing process monitoring with a biaxially oriented polypropylene film based fiber Fabry-Perot sensor, Opt. Commun. 475 (2020), 126292.
[28] M. Fajkus, J. Nedoma, R. Martinek, J. Brablik, J. Vanus, M. Novak, et al., MR Fully compatible and safe FBG breathing sensor: a practical solution for respiratory triggering, IEEE Access 7 (2019) 123013–123025.
[29] S. Pant, S. Umesh, S. Asokan, "Fiber Bragg Grating Respiratory Measurement Device," in *2018 IEEE International Symposium on Medical Measurements and Applications (MeMeA)*, 2018, pp. 1-5.
[30] L. Mohanty, K.S.C. Kuang, A breathing rate sensor with plastic optical fiber, Appl. Phys. Lett. 97 (2010), 073703.
[31] C. Zhao, D. Liu, Z. Cai, B. Du, M. Zou, S. Tang, et al., A wearable breath sensor based on fiber-tip microcantilever, Biosensors 12 (2022) 168.
[32] X. Li, D. Liu, R. Kumar, W.P. Ng, Y.-Q. Fu, J. Yuan, et al., A simple optical fiber interferometer based breathing sensor, Meas. Sci. Technol. 28 (2017), 035105.
[33] A.C. Nepomuceno, T. Paixão, N. Alberto, P.S.d.B. André, P. Antunes, M. F. Domingues, Optical fiber fabry-perot interferometer based spirometer: design and performance evaluation, *Photonics* 8 (2021) 336.
[34] A. Aitkulov, D. Tosi, Design of an all-POF-fiber smartphone multichannel breathing sensor with camera-division multiplexing, IEEE Sens. Lett. 3 (2017) 1–4.
[35] H. Yu, Z. Luo, Y. Zheng, J. Ma, X. Jiang, D. Jiang, Vibration sensing using liquid-filled photonic crystal fiber with a central air-bore, J. Lightwave Technol. 37 (2019) 4625–4633.
[36] E. Mansour, R. Vishinkin, S. Rihet, W. Saliba, F. Fish, P. Sarfati, et al., Measurement of temperature and relative humidity in exhaled breath, Sens. Actuators, B 304 (2020), 127371.

[37] P. Höppe, Temperatures of expired air under varying climatic conditions, Int. J. Biometeorol. 25 (1981) 127–132.
[38] J. Cheng, L. Zhang, K. Zhao, Y. Wang, X. Cao, S. Zhang, et al., Flexible multifunctional photonic crystal fibers with shape memory capability for optical waveguides and electrical sensors, Ind. Eng. Chem. Res. 60 (2021) 8442–8450.
[39] A. Manujło, T. Osuch, *Temperature fiber Bragg grating based sensor for respiration monitoring* vol. 10445: SPIE, 2017.
[40] W.-J. Yoo, K.-W. Jang, J.-K. Seo, J.-Y. Heo, J.-S. Moon, J.-Y. Park, et al., Development of respiration sensors using plastic optical fiber for respiratory monitoring inside MRI system, J. Opt. Soc. Korea 14 (2010) 235–239.
[41] W. Chen, Y. Zhang, H. Yang, Y. Qiu, H. Li, Z. Chen, et al., Non-invasive measurement of vital signs based on seven-core fiber interferometer, IEEE Sens. J. 21 (2021) 10703–10710.
[42] M. Fajkus, J. Nedoma, R. Martinek, V. Vasinek, H. Nazeran, P. Siska, A non-invasive multichannel hybrid fiber-optic sensor system for vital sign monitoring, Sensors 17 (2017) 111.
[43] Y. Koyama, M. Nishiyama, K. Watanabe, Smart textile using hetero-core optical fiber for heartbeat and respiration monitoring, IEEE Sens. J. 18 (2018) 6175–6180.
[44] L. Liang, H. Sun, N. Liu, H. Luo, T. Gang, Q. Rong, et al., High-sensitivity optical fiber relative humidity probe with temperature calibration ability, Appl. Opt. 57 (2018) 872–876.
[45] L. Liu, S.P. Morgan, R. Correia, S. Korposh, A single-film fiber optical sensor for simultaneous measurement of carbon dioxide and relative humidity, Opt. Laser Technol. 147 (2022), 107696.
[46] D. Lo Presti, A. Carnevale, J. D'Abbraccio, L. Massari, C. Massaroni, R. Sabbadini, et al., A multi-parametric wearable system to monitor neck movements and respiratory frequency of computer workers, Sensors 20 (2020) 536.
[47] K. Ogawa, S. Koyama, H. Ishizawa, S. Fujiwara, K. Fujimoto, "Simultaneous Measurement of Heart Sound, Pulse Wave and Respiration with Single Fiber Bragg Grating Sensor," in *2018 IEEE International Symposium on Medical Measurements and Applications (MeMeA)*, 2018, pp. 1-5.
[48] D.L. Presti, C. Massaroni, J. D'Abbraccio, L. Massari, M. Caponero, U.G. Longo, et al., Wearable system based on flexible FBG for respiratory and cardiac monitoring, IEEE Sens. J. 19 (2019) 7391–7398.
[49] F.D. Tommasi, C. Massaroni, A. Carnevale, D.L. Presti, E.D. Vita, A. Iadicicco, et al., Fiber bragg grating sensors for temperature monitoring during thermal ablation procedure: experimental assessment of artefact caused by respiratory movements, IEEE Sens. J. 21 (2021) 13342–13349.
[50] S. Kano, N. Jarulertwathana, S. Mohd-Noor, J.K. Hyun, R. Asahara, H. Mekaru, Respiratory monitoring by ultrafast humidity sensors with nanomaterials: a review, Sensors 22 (2022) 1251.
[51] A.M. Shrivastav, D.S. Gunawardena, Z. Liu, H.-Y. Tam, Microstructured optical fiber based Fabry-Pérot interferometer as a humidity sensor utilizing chitosan polymeric matrix for breath monitoring, Sci. Rep. 10 (2020) 6002.
[52] W. Yuan, L. Li, Y. Wang, Z. Lian, D. Chen, C. Yu, et al., Temperature and curvature insensitive all-fiber sensor used for human breath monitoring, Opt. Express 29 (2021) 26375–26384.
[53] R. Sinha, F.U. Hernandez, C. He, S. Korposh, R. Correia, A.M. Norris, et al., Development and validation of a novel fibre-optic respiratory rate sensor (FiRRS) integrated in oxygen delivery devices, J. Phys. D Appl. Phys. 54 (2021), 124002.
[54] D.L. Presti, C. Massaroni, M. Zaltieri, R. Sabbadini, A. Carnevale, J.D. Tocco, et al., A magnetic resonance-compatible wearable device based on functionalized fiber optic sensor for respiratory monitoring, IEEE Sens. J. 21 (2021) 14418–14425.
[55] L. Chen, B. Liu, J. Liu, J. Yuan, H.P. Chan, T. Wu, et al., U-shape panda polarization-maintaining microfiber sensor coated with graphene oxide for relative humidity measurement, J. Lightwave Technol. 39 (2021) 6308–6314.
[56] B. Jiang, Z. Bi, Z. Hao, Q. Yuan, D. Feng, K. Zhou, et al., Graphene oxide-deposited tilted fiber grating for ultrafast humidity sensing and human breath monitoring, Sens. Actuators, B 293 (2019) 336–341.
[57] C. Massaroni, D.L. Presti, P. Saccomandi, M.A. Caponero, R. D'Amato, E. Schena, Fiber bragg grating probe for relative humidity and respiratory frequency estimation: assessment during mechanical ventilation, IEEE Sens. J. 18 (2018) 2125–2130.
[58] C. Massaroni, D.L. Presti, C. Losquadro, P. Resta, P. Saccomandi, E. Schena, *et al.*, "Multi-sensitive FBG-based needle for both relative humidity and breathing rate monitoring," in *2018 IEEE International Symposium on Medical Measurements and Applications (MeMeA)*, 2018, pp. 1-6.
[59] A. Lopez Aldaba, D. Lopez-Torres, C. Elosua, J.L. Auguste, R. Jamier, P. Roy, et al., SnO2-MOF-Fabry-Perot optical sensor for relative humidity measurements, Sens. Actuators, B 257 (2018) 189–199.
[60] D. Li, H. Lu, W. Qiu, J. Dong, H. Guan, W. Zhu, et al., Molybdenum disulfide nanosheets deposited on polished optical fiber for humidity sensing and human breath monitoring, Opt. Express 25 (2017) 28407–28416.
[61] Y. Wang, J. Wang, Y. Shao, C. Liao, Y. Wang, Highly sensitive surface plasmon resonance humidity sensor based on a polyvinyl-alcohol-coated polymer optical fiber, Biosensors 11 (2021) 461.
[62] J. Wang, Surface plasmon resonance humidity sensor based on twisted long period fiber grating coated with tungsten disulfide film, Optik 236 (2021), 166616.
[63] B. Du, D. Yang, Y. Ruan, P. Jia, H. Ebendorff-Heidepriem, Compact plasmonic fiber tip for sensitive and fast humidity and human breath monitoring, Opt. Lett. 45 (2020) 985–988.
[64] M. Hernaez, B. Acevedo, A.G. Mayes, S. Melendi-Espina, High-performance optical fiber humidity sensor based on lossy mode resonance using a nanostructured polyethylenimine and graphene oxide coating, Sens. Actuators, B 286 (2019) 408–414.
[65] W. Chen, Z. Chen, Y. Zhang, H. Li, Y. Lian, Agarose coated macro-bend fiber sensor for relative humidity and temperature measurement at 2 μm, Opt. Fiber Technol. 50 (2019) 118–124.
[66] X. Zhang, X. Zhang, Y. Zhang, W. Peng, In-fibre micro-channel: its potential for in-fibre detection, Analyst 147 (2022) 828–833.
[67] M. Shao, R. Zhang, X. Zhao, W. Zhang, Q. Lu, X. Qiao, Dual-core fiber based in-line Michelson interferometer for humidity sensing, Opt. Fiber Technol. 64 (2021), 102570.
[68] Z. Hu, Y. Chen, J. Tan, Z. Yan, Z. Weng, M. Gusain, et al., A hybrid self-growing polymer microtip for ultracompact and fast fiber humidity sensing, Sens. Actuators, B 346 (2021), 130462.
[69] W. Bao, F. Chen, H. Lai, S. Liu, Y. Wang, Wearable breath monitoring based on a flexible fiber-optic humidity sensor, Sens. Actuators, B 349 (2021), 130794.
[70] Y. Liu, H. Lin, Y. Dai, A. Zhou, L. Yuan, Humidity sensor based on an in-fiber integrated Mach-Zehnder interferometer, IEEE Photonics Technol. Lett. 31 (2019) 393–396.
[71] M. Shao, H. Sun, J. Liang, L. Han, D. Feng, In-fiber michelson interferometer in photonic crystal fiber for humidity measurement, IEEE Sens. J. 21 (2021) 1561–1567.
[72] Y. Xu, Z. Zhou, Y. Guo, L. Liu, Y. Xu, C. Qiao, et al., Carbon dioxide detection using polymer-coated fiber Bragg grating based on volume dilation mechanism and molecular dynamics simulation, Appl. Surf. Sci. 584 (2022), 152616.
[73] J. Hromadka, B. Tokay, R. Correia, S.P. Morgan, S. Korposh, Carbon dioxide measurements using long period grating optical fibre sensor coated with metal organic framework HKUST-1, Sens. Actuators, B 255 (2018) 2483–2494.
[74] L. Liu, S.P. Morgan, R. Correia, S.-W. Lee, S. Korposh, Multi-parameter optical fiber sensing of gaseous ammonia and carbon dioxide, J. Lightwave Technol. 38 (2020) 2037–2045.
[75] W. Ma, J. Xing, R. Wang, Q. Rong, W. Zhang, Y. Li, et al., Optical fiber Fabry-Perot interferometric CO_2 gas sensor using guanidine derivative polymer functionalized layer, IEEE Sens. J. 18 (2018) 1924–1929.
[76] T. Katagiri, K. Shibayama, T. Iida, Y. Matsuura, Infrared hollow optical fiber probe for localized carbon dioxide measurement in respiratory tracts, Sensors 18 (2018) 995.
[77] J. Moll, V. Wright, An objective clinical study of chest expansion, Ann. Rheum. Dis. 31 (1972) 1.
[78] J. Li, B. Liu, J. Liu, J.-L. Shi, X.-D. He, J. Yuan, et al., Low-cost wearable device based D-shaped single mode fiber curvature sensor for vital signs monitoring, Sens. Actuators, A 337 (2022), 113429.
[79] J.D. Tocco, D.L. Presti, M. Zaltieri, G. D'Alesio, M. Filosa, L. Massari, et al., A wearable system based on flexible sensors for unobtrusive respiratory monitoring in occupational settings, IEEE Sens. J. 21 (2021) 14369–14378.
[80] Y.N. Pang, B. Liu, J. Liu, S.P. Wan, T. Wu, X. He, et al., Wearable optical fiber sensor based on a bend singlemode-multimode-singlemode fiber structure for respiration monitoring, IEEE Sens. J. 21 (2021) 4610–4617.
[81] K. Chethana, A.S. Guru Prasad, S.N. Omkar, S. Asokan, Fiber bragg grating sensor based device for simultaneous measurement of respiratory and cardiac activities, J. Biophotonics 10 (2017) 278–285.
[82] C. Massaroni, P. Saccomandi, D. Formica, D.L. Presti, M.A. Caponero, G.D. Tomaso, et al., Design and feasibility assessment of a magnetic resonance-compatible smart textile based on fiber Bragg grating sensors for respiratory monitoring, IEEE Sens. J. 16 (2016) 8103–8110.
[83] A. Issatayeva, A. Beisenova, D. Tosi, C. Molardi, Fiber-optic based smart textiles for real-time monitoring of breathing rate, Sensors 20 (2020) 3408.
[84] T. Li, Y. Su, F. Chen, X. Liao, Q. Wu, Y. Kang, et al., A skin-like and highly stretchable optical fiber sensor with the hybrid coding of wavelength-light intensity, Adv. Intell. Syst. (2021) 2100193.
[85] A.G. Leal-Junior, C.R. Díaz, C. Leitão, M.J. Pontes, C. Marques, A. Frizera, Polymer optical fiber-based sensor for simultaneous measurement of breath and heart rate under dynamic movements, Opt. Laser Technol. 109 (2019) 429–436.
[86] D. Ahn, Y.J. Park, J.-D. Shin, J. Lee, J. Park, Plastic optical fiber respiration sensor based on in-fiber microholes, Microwave Opt. Technol. Lett. 61 (2019) 120–124.
[87] D. Sartiano, S. Sales, Low cost plastic optical fiber pressure sensor embedded in mattress for vital signal monitoring, Sensors 17 (2017) 2900.
[88] I. Sadek, T.T.S. Heng, E. Seet, B. Abdulrazak, A new approach for detecting sleep apnea using a contactless bed sensor: comparison study, J. Med. Internet Res. 22 (2020) e18297.
[89] Y. Wang, M. You, Y. Zhang, S. Wu, Y. Zhang, H. Yang, et al., Noninvasive measurement of the vital signs of cancer patients with a dual-path microbend fiber sensor, Biomed. Opt. Express 13 (2022) 982–994.
[90] J. Pan, C. Jiang, Z. Zhang, L. Zhang, X. Wang, L. Tong, Flexible liquid-filled fiber adapter enabled wearable optical sensors, Adv. Mater. Technol. 5 (2020) 2000079.
[91] F. Tan, S. Chen, W. Lyu, Z. Liu, C. Yu, C. Lu, et al., Non-invasive human vital signs monitoring based on twin-core optical fiber sensors, Biomed. Opt. Express 10 (2019) 5940–5952.
[92] R. Wang, J. Zhao, Y. Sun, H. Yu, N. Zhou, H. Zhang, et al., Wearable respiration monitoring using an in-line few-mode fiber Mach-Zehnder interferometric sensor, Biomed. Opt. Express 11 (2020) 316–329.
[93] S. Wang, X. Ni, L. Li, J. Wang, Q. Liu, Z. Yan, et al., Noninvasive monitoring of vital signs based on highly sensitive fiber optic mattress, IEEE Sens. J. 20 (2020) 6182–6190.
[94] H.-F. Hu, S.-J. Sun, R.-Q. Lv, Y. Zhao, Design and experiment of an optical fiber micro bend sensor for respiration monitoring, Sens. Actuators, A 251 (2016) 126–133.
[95] M. Roudjane, S. Bellemare-Rousseau, E. Drouin, B. Bélanger-Huot, M.A. Dugas, A. Miled, et al., Smart T-shirt based on wireless communication spiral fiber sensor

array for real-time breath monitoring: validation of the technology, IEEE Sens. J. 20 (2020) 10841–10850.